J. Phys.: Condens. Matter 7 (1995) 5289–5301. Printed in the UK

Structural rearrangement and surface magnetism on oxide surfaces: a temperature-dependent low-energy electron diffraction–electron energy loss spectroscopy study of $Cr_2O_3(111)/Cr(110)$

M Bender†, D Ehrlich†, I N Yakovkin†§, F Rohr†, M Bäumer†, H Kuhlenbeck†, H-J Freund† and V Staemmler‡

† Lehrstuhl für Physikalische Chemie I, Ruhr-Universität Bochum, D-44780 Bochum, Germany

‡ Lehrstuhl für Theoretische Chemie, Ruhr-Universität Bochum, D-44780 Bochum, Germany

Received 3 April 1995

Abstract. Structural rearrangements of the (111) surface in the system $Cr_2O_3/Cr(110)$ as a function of temperature were investigated by means of low-energy electron diffraction (LEED) and electron energy loss spectroscopy (EELS). At room temperature, one observes a simple (1 × 1) LEED pattern of the clean (111) surface. If the temperature was lowered to 150 K a $(\sqrt{3} \times \sqrt{3})R30^{\circ}$ superstructure was observed. The structure reached its maximum intensity at about 150 K substrate temperature. Below 150 K the superstructure vanished again and the simple (1 × 1) LEED pattern of the (111) surface was recovered at 90–100 K. Parallel to this, a considerable change in the electron energy loss spectra with varying temperature was observed. With the help of quantum-chemical cluster calculations the low-energy excitations in the range between 0.8 and 2.5 eV were assigned to local d–d excitations of Cr^{3+} ions at the $Cr_2O_3(111)$ surface. Some of these peaks were quenched upon adsorption of gases such as CO, NO or CO_2. We propose a model of two successive phase transitions the first of which is a disorder-to-order transition above 150 K whereas the second is an order-to-order transition below 150 K. The transitions may be driven by antiferromagnetic coupling of the surface chromium ions to those in the second layer.

1. Introduction

Oxide surfaces have received increasing attention in recent years [1–4]. Most investigations have concentrated on the non-polar surfaces, which are often (e.g. in the case of the rock salt structures) the thermodynamically stable surfaces. Only a few studies deal with the polar non-stable surfaces. One example from our laboratory has been the water-induced deconstruction of the octopolar reconstructed polar NiO(111) surface [5]. In this case the structural rearrangement involves three layers of the oxide. The mass transport involved leads to a relatively disordered surface indicated by diffuse low-energy electron diffraction (LEED) superstructure spots. There are other polar oxide surfaces, however, where the creation of the most stable surface does not involve more than the top layer [1, 6–9]. For example, the (111) surface of Cr_2O_3 (figure 1(*b*)) may be created by cutting the crystal perpendicular to the (111) direction along a plane dividing the buckled plane of Cr^{3+} ions

§ Permanent address: Institute of Physics, Ukrainian Academy of Science, Prospekt Nauki 46, Kiev 252028, Ukraine.

0953-8984/95/275289+13$19.50

such that half of the Cr^{3+} ions remain on each side of the cutting plane. Figure 1(*b*) shows the resulting surface structure. There are three possible positions for the Cr^{3+} ions on the surface (site 1, site 2 and site 3), not all of which are occupied in a bulk terminated structure and it is not at all clear that the position corresponding to the bulk structure is the most stable site for the Cr^{3+} ions on the surface. Via a simple site-hopping mechanism involving the nearest-neighbour position, one structure could be driven into the other structure. We have investigated the surface structure via LEED as a function of temperature and find indications of structural rearrangements. An interesting question that may be asked in this connection is what role surface magnetism could play in stabilizing the various structures. The magnetic properties of bulk transition-metal oxides have been studied in great detail [10, 11] but the consequences for surface structure have not been elucidated up to now. It is well known for example in the case of bulk oxides that the onset of antiferromagnetism below the Néel temperature leads to a small distortion of the crystal lattice [11].

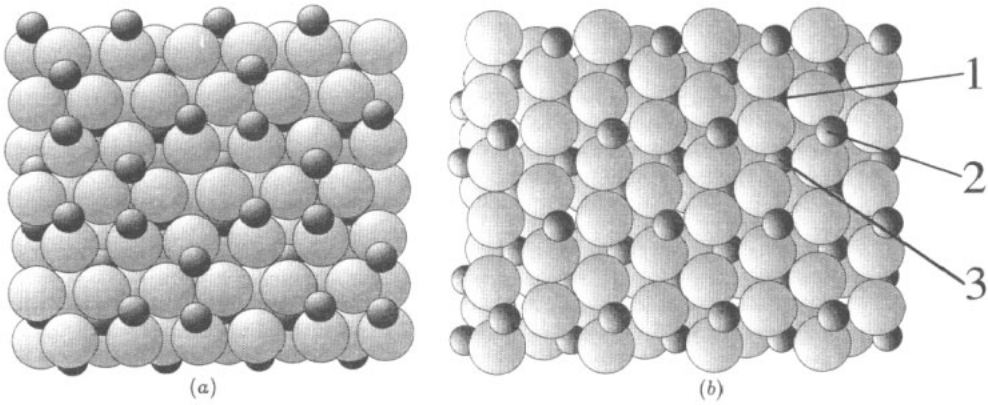

Figure 1. (*a*) Side view of the Cr_2O_3 structure perpendicular to the (111) direction. (*b*) (111) surface of the Cr_2O_3 crystal cutting the buckled Cr^{3+} ion plane in two halves. The three possible sites 1, 2 and 3 for the Cr^{3+} ions are indicated.

In the present work we shall present experimental evidence for a structural reconstruction of a $Cr_2O_3(111)$ surface dependent on temperature as evidenced by LEED and electron energy loss spectroscopy (EELS) data. We shall discuss magnetic coupling between the top and the second chromium ion layer as the source of this reconstruction.

2. Experiment set-up

The experiments were carried out in two different UHV chambers. The one used for the LEED experiments has already been described elsewhere [12]. The equipment consists of a VSW x-ray photoelectron spectrometer, a conventional Omikron LEED system and a sputter gun for the preparation of the samples. The electron energy loss (EEL) spectra were taken in a separate chamber [13] with an EEL spectrometer set to 150 meV resolution.

The chromium oxide film was prepared similar to the procedure described in [14, 15]. A chromium metal single-crystal surface with (110) orientation as polished *ex vacuo* was inserted into the UHV and cleaned by argon ion bombardment until any nitrogen

contamination was removed. The clean metal surface was oxidized by exposing it for 1 min at 540 K and for 2 min at 780 K to an oxygen pressure of 2×10^{-6} Torr. Before each measurement the sample was cleaned by flashing to 1000–1050 K under base pressure conditions of 2×10^{-10} Torr. The temperature of the sample was measured with a Ni-(Cr-Ni) thermocouple with reference to room temperature (25 °C).

3. Low-energy electron diffraction investigations

The freshly prepared oxide surface was cleaned by flashing to 1000 K. While the sample was cooling, its LEED structure (figure 2) was photographed. At room temperature the main diffraction spots spanned a simple hexagon (figure 2(a)). Additionally, a hexagonal diffuse patch surrounding the (0,0) diffraction spot was observed. Upon cooling, the diffuse intensity transformed into a $(\sqrt{3} \times \sqrt{3})R30°$ superstructure, showing its maximum intensity at about 150 K (figure 2(b)). Below this temperature the superstructure vanished again and finally a simple hexagonal LEED pattern without any additional structure was recovered (figure 2(c)). The whole temperature dependence was reversible, i.e. it could be observed also when the sample was warmed starting at 90 K.

Figure 3 contains a plot of the intensity within an area indicated in the inset around the first-order superstructure spot as a function of temperature. It is quite clear that the transition towards a lower temperature leads to the disappearance of the superstructure spot, while the transition towards a higher temperature leads only to a partial loss in intensity but an increased diffuseness of the superstructure. This is a strong indication that we are dealing with an order-to-order transition at low temperatures and an order-to-disorder transition towards higher temperatures.

Also, the superstructure showed a pronounced sensitivity to the adsorption of various molecular species. At the maximum intensity of the superstructure, i.e. at about 150 K, the sample was exposed to carbon dioxide (pressure, (5–8) $\times 10^{-8}$ Torr) which is known to chemisorb strongly on the chromium oxide surface [7]. The superstructure is quenched immediately after the onset of exposure. It could only be recovered by flashing the sample to the temperature at which thermal desorption of the corresponding species takes place, i.e. about 400 K for carbon dioxide.

From these adsorption experiments we conclude that the structural rearrangement on the clean sample takes place directly at the surface and that the interaction between the adsorbates and the substrate strongly influences the energetics of the structural rearrangement at the surface.

4. Electron energy loss spectra

Figure 4 shows EEL spectra taken from the clean flashed oxide surface at different temperatures. At 90 K the spectrum exhibits two signals at loss energies of about 1.2 eV and about 1.4 eV, denoted by A and B, respectively. They are accompanied by a broad feature C at about 1.8 eV. As the temperature rises, signals A and B lose intensity whereas the intensity of feature C increases. All three signals A, B and C lie in the regime of d–d transitions of chromium ions [16, 6] and we shall present a detailed assignment further below.

Figure 5 shows the EEL spectrum of the clean chromium oxide surface at 90–100 K compared to spectra of the same surface after exposure to different gases. The spectrum

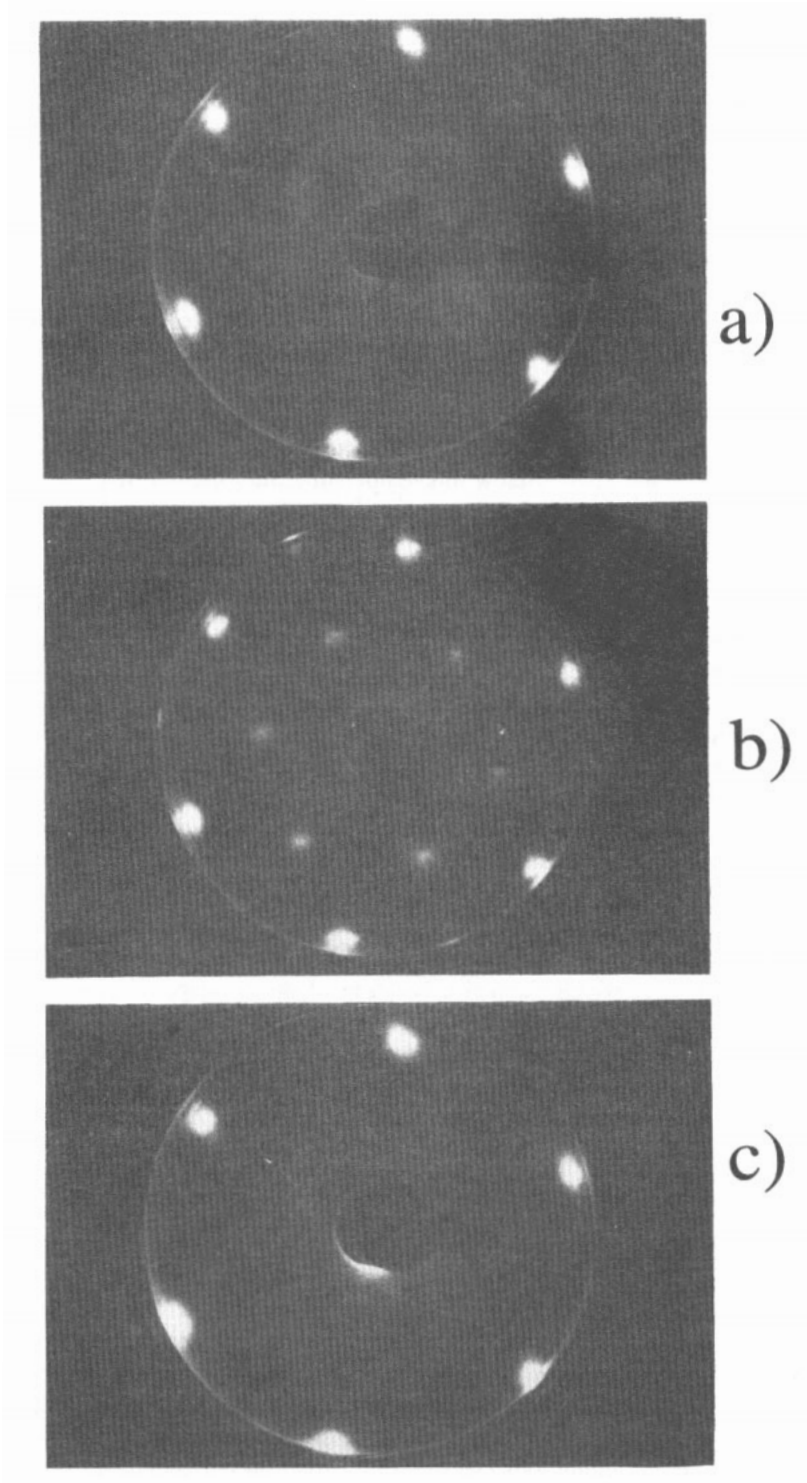

Figure 2. LEED photographs (primary energy, 23.7 ± 0.1 eV) of the chromium oxide $Cr_2O_3(111)/Cr(110)$ surface after flash to 1000 K taken at different temperatures: (a) about 300 K; (b) about 150 K; (c) about 90–100 K.

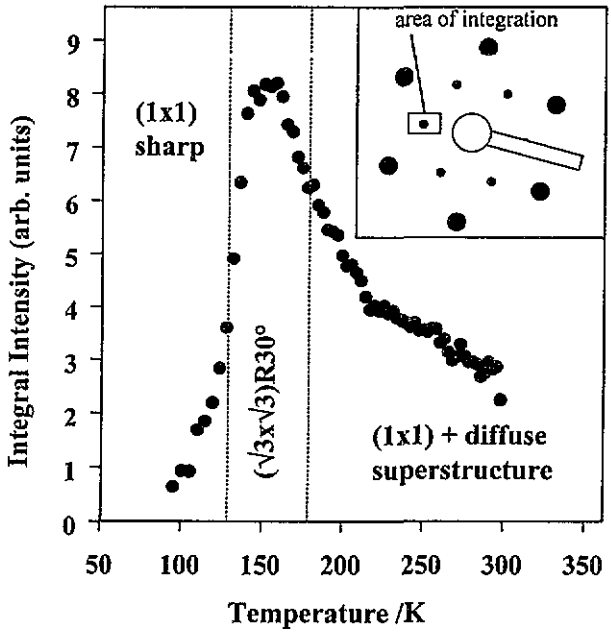

Figure 3. Temperature dependence of the first-order superstructure spot intensity of the $(\sqrt{3}\times\sqrt{3})R30°$ superstructure. The inset indicates the area in reciprocal space used for intensity determination.

in the considered energy region changes dramatically when various adsorbates are present. Thus we assign signals A–C to d–d transitions of surface chromium ions which are sensitive to the presence of adsorbates. Feature C may also contain some intensity of d–d excitations of bulk chromium ions in a distorted octahedral crystal field. This assignment is supported by optical spectra of bulk chromium oxide samples [17] as well as of ruby crystals [18] and is also in line with the observation that in the range of feature C some intensity remains after adsorption. Parallel to the temperature dependence of the LEED data we also observe a temperature dependence of the EELS data as shown in figure 4, where we see a change in the intensity distribution for peaks A, B and C. Let us assume for the moment that the thermodynamics of the surface processes are appropriately described by a Boltzmann distribution (which could be debated). Then we can use the measured temperature dependence of the system and plot the logarithm of the quotient of intensities of feature A and feature C versus $1/T$, which results in figure 6. From the slope we may estimate an energy difference of 7 meV between the state of the surface characterized by feature A and the state of the surface characterized by feature C [19]. This energy is of the order of magnetically dominated interactions.

5. Cluster calculations

In order to check this assignment we have performed a series of quantum-chemical *ab initio* cluster calculations for the ground state and the first electronic excited states of chromium ions in bulk Cr_2O_3 and at the $Cr_2O_3(111)$ surface. Our cluster consists of one Cr^{3+} ion surrounded either by six O^{2-} ions which form a slightly distorted octahedron (bulk Cr_2O_3)

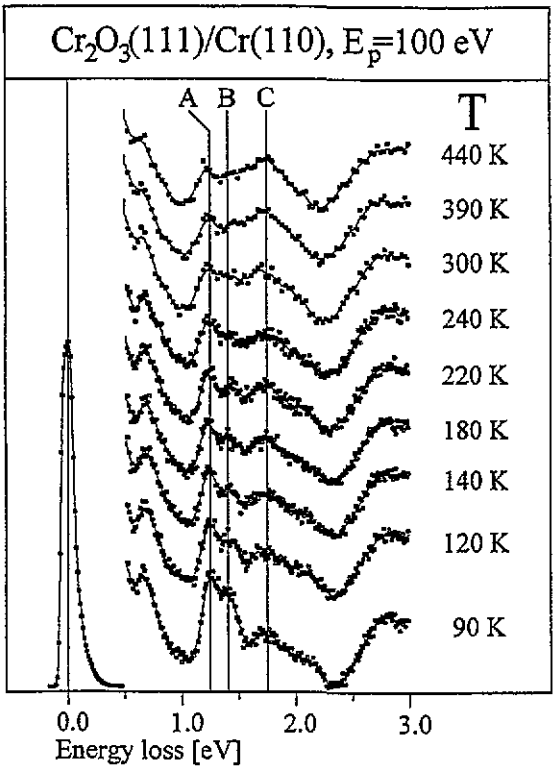

Figure 4. EEL spectra of the clean flashed chromium oxide surface at different temperatures. The spectra were taken in specular detection at 100 eV primary energy of the incident electrons. The resolution was set to about 150 meV as can be seen from the FWHM of the no-loss signal. The three signals mentioned in the text are denoted as A (about 1.2 eV), B (1.4 eV) and C (1.8 eV) respectively.

or by three O^{2-} ions which represent the next neighbours of a Cr^{3+} ion at the (111) surface. This cluster is embedded in an infinite or semi-infinite field of point charges +3e and −2e which simulate the Madelung field of the Cr_2O_3 ionic crystal. Within both the cluster and the point charge field the experimental crystal structure of bulk Cr_2O_3 [20] was used. The present *ab initio* calculations were performed at the complete active space self-consistent field (CASSCF) and valence configuration interaction (VCI) levels in the same way as in our previous study of surface states in NiO [21] and CoO [22, 23]. The results of our calculations, together with the experimental EELS data, are summarized in figure 7.

Cr^{3+} is a d^3 system, and its electronic ground state in the gas phase is a ^4F state which is split in an octahedral crystal field into a $^4A_{2g}$ ground state, a first excited $^4T_{2g}$ and a second excited $^4T_{1g}$ state. The threefold spatial degeneracies of the excited states of T_{2g} and T_{1g} symmetry are further split (by about 0.02 eV) in the slightly distorted octahedral crystal field of bulk Cr_2O_3. The lowest excitation energies are calculated at the CASSCF level to be 1.73 eV ($^4T_{2g}$) and 2.73 eV ($^4T_{1g}$) which compares quite favourably with the optical absorption data of 2.0 and 2.8 eV [17]. Our first excitation energy is too low, possibly because the ligand field strength 10Dq generated by the cluster in the Madelung field is too small. Similar calculations for the $Cr^{3+}(H_2O)_6$ complex are in line with this observation.

We have not included the lowest doublet state (^2E in octahedral symmetry, which is

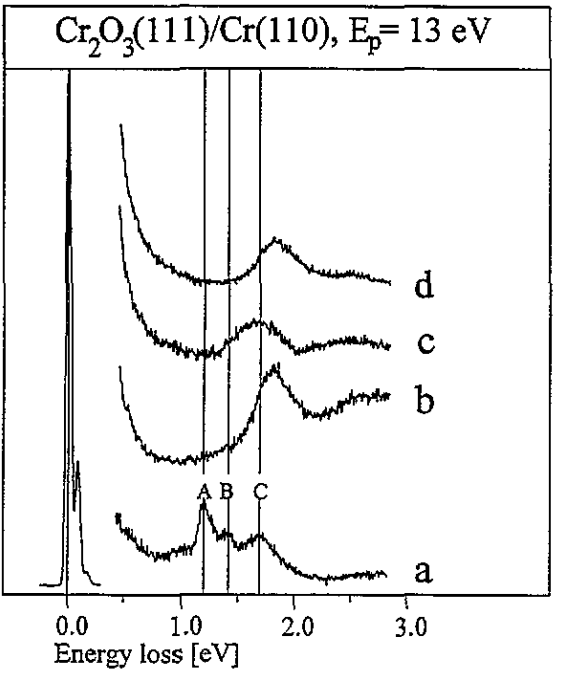

Figure 5. EEL spectra of the chromium oxide $Cr_2O_3(111)/Cr(110)$ surface after flash to about 1000 K and cooling to 90 K: curve (a), without adsorbate; curve (b), after adsorption of CO; curve (c), after adsorption of NO; curve (d), after adsorption of CO_2.

the lowest component of the ^2G state of the free Cr^{3+} ion) in figure 7 since firstly it cannot be described properly at the CASSCF level because it is stabilized by about 0.5 eV by dynamical correlation effects which are not included in our CASSCF calculations and secondly its energy relative to the $^4A_{2g}$ ground state at about 1.85 eV [16] is not affected by the ligand field and therefore nearly identical in various Cr^{3+} complexes, in bulk Cr_2O_3 and at the $Cr_2O_3(111)$ surface.

At the $Cr_2O_3(111)$ surface the Cr^{3+} ions are exposed to a weaker crystal field since half the oxygen ions are removed. Furthermore, this field has only (distorted) C_{3v} symmetry compared to the higher O_h symmetry in bulk Cr_2O_3. Therefore, one can expect that the energy differences between the components of ^4F are smaller at the surface than in the bulk and that the quasi-degeneracies of the T_{2g} and the T_{1g} levels are split. Figure 7 shows our CASSCF results for the three non-equivalent Cr^{3+} ions at the $Cr_2O_3(111)$ surface (sites 1, 2 and 3 in figure 1) and confirms this expectation. For all three positions both the $^4T_{2g}$ and the $^4T_{1g}$ states are lowered considerably relative to the $^4A_{2g}$ ground state and are slightly split ($^4T_{2g}$ into $^4A_1$ and ^4E; $^4T_{1g}$ into $^4A_2$ and ^4E). Despite these similarities, the d–d spectra of the Cr^{3+} ions at the three non-equivalent sites differ to some extent. Due to the weaker ligand fields, the Cr^{3+} ions at sites 2 and 3 have considerably smaller excitation energies (the lowest at about 0.9 eV and 1.5 eV) than at site 1 (1.05 eV and 1.26 eV). If we assume that the calculated excitation energies of the components of $^4T_{2g}$ are too low by 0.1–0.2 eV, the d–d excitation energies for the Cr^{3+} at site 1 are in reasonable agreement with the measured EEL spectra, while those of the Cr^{3+} ions at sites 2 and 3 are considerably lower.

In these calculations the Cr^{3+} ions have been given fixed positions. For the two sites occupied in the bulk, the choice could be based on those interatomic distances known from

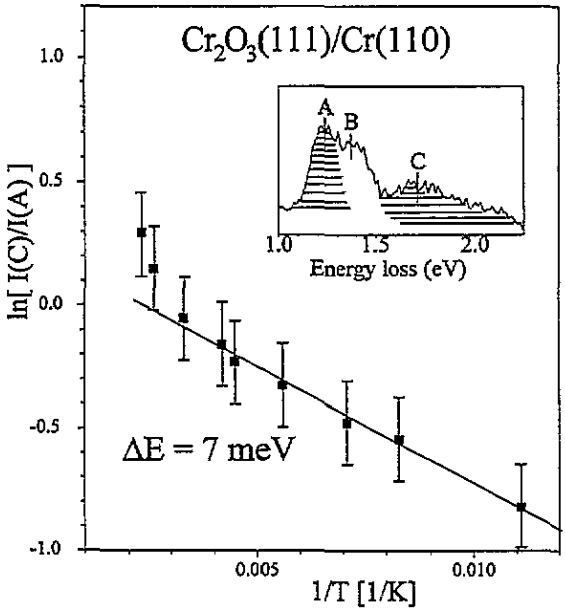

Figure 6. Temperature dependence of the chromium oxide $Cr_2O_3(111)/Cr(110)$ surface states as analysed from figure 4. The inset shows the areas under peaks A and C, respectively, which have been taken into account for the data analysis. The error bars represent the uncertainty in locating the maxima and the straight line is meant to guide the eye.

the bulk; for the third position which is not occupied in the bulk, a reasonable position has been assumed.

If one allows for geometry relaxation, one observes a very interesting effect, the Cr^{3+} ion residing in site 1 exhibits a stable geometry with internuclear distances very near the bulk values. Its equilibrium position is moved slightly (by 0.15 Å) towards the oxygen layer, accompanied by a slight increase in the lowest d–d excitation energies to 1.23 and 1.39 eV in nearly perfect agreement with the EELS data. The Cr^{3+} in site 2 is not stable with respect to motion below the oxygen plane. Once the ion has moved below the oxygen plane, the electrostatic repulsive interaction increases. Therefore the Cr^{3+} ions will have a tendency to avoid site 2. Site 3 is not populated in bulk Cr_2O_3; however, it is stable with respect to motion of the Cr^{3+} ions below the oxygen plane because in this case the site below is occupied by another Cr^{3+} ion.

The interpretation of the EEL spectra of figures 4 and 5 by means of the CASSCF results in figure 7 is straightforward. The high-energy part of the broad signal C between 1.7 and 2.2 eV contains certainly the $^4T_{2g}$ state of bulk Cr_2O_3 and the ^4E surface component of the $^4T_{1g}$ state of a Cr^{3+} ion at site 1. At 300 K the low-energy part of signal C is mainly attributed to the surface components of the $^4T_{2g}$ state ($^4A_1$ and ^4E) of the ions at site 3. It probably contains also the intensity of the ^2E bulk state which is not included in our calculations. Finally, the signals A and B are definitely the surface states correlating with the first excited $^4T_{2g}$ of bulk Cr_2O_3. Most probably, the double peak is to be attributed to the two components ($^4A_1$ and ^4E) of $^4T_{2g}$ split in the C_{3v} symmetry at the surface at site 1.

We have also performed similar CASSCF calculations for Cr^{2+} ions in the same positions at the surface. The excitation energies are 0.7 and 2.0 eV (site 2) and 0.8 and 2.0 eV (site 1), respectively, for the lowest excited $^5T_{1g}$ and $^3T_{2g}$ states; they show no similarity to

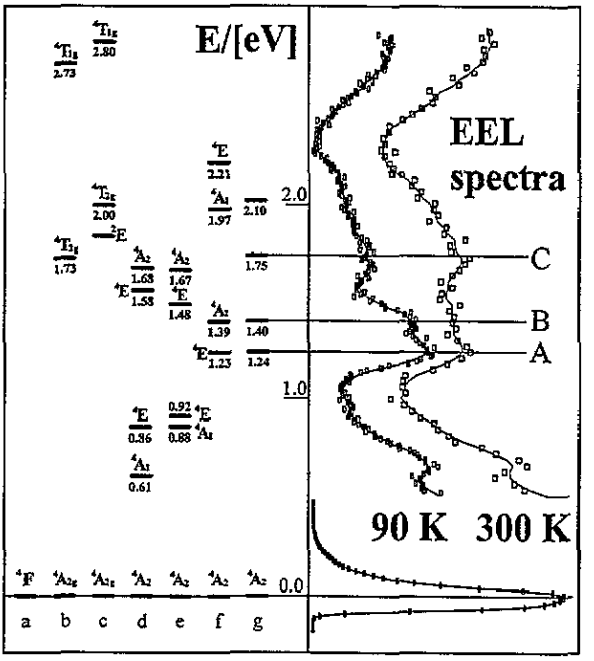

Figure 7. Experimental and CASSCF results for the lowest electronic states for bulk Cr_2O_3 and at the $Cr_2O_3(111)$ surface, where the spectra have been copied from figure 4: (a), free Cr^{3+} ion; (b), bulk, CASSCF; (c), bulk, experimental results [17]; (d), surface, site 3; (e), surface, site 2; (f), surface, site 1, relaxed geometry; (g), EELS, this work.

the observed EEL spectrum. Thus, the previous suggestion [6, 7] that the signals A and B have to be attributed to Cr^{2+} ions at the surface is not supported by the present calculations. However, as is shown elsewhere [24], the adsorption of Na onto the $Cr_2O_3(111)$ leads to the formation of Cr^{2+} on the surface.

6. Discussion

In the following we shall propose a model which explains the structural changes on the clean chromium oxide surface. We shall start with a model for the system at 90–100 K and then consider mechanisms possibly involved in the phase transition.

Figures 8(a)–(c) show truncations of the bulk α-corundum-type chromium oxide crystal structure [20] parallel to the (111) plane with three different possible terminations. Figure 8(a) shows the termination by oxygen ions and figure 8(b) the termination by a complete buckled chromium ion layer. In both cases the surface is electrostatically unstable. However, if only half the Cr^{3+} ions remain on the surface, as alluded to in the introduction, the resulting charge density on the surface is reduced to half its value in figure 8(b). This surface is electrostatically stable [25]. The lattice vectors were calculated from the LEED pattern by comparison to the LEED pattern of the clean chromium metal lattice [10].

We consider the low-temperature (90 K) phase to be the ideal $Cr_2O_3(111)$ surface with half a layer of Cr^{3+} ions present at the surface as shown in figure 8(c) exhibiting a (1×1) LEED pattern (figure 2(c)). Upon raising the temperature above 100 K, a $(\sqrt{3} \times \sqrt{3})R30°$

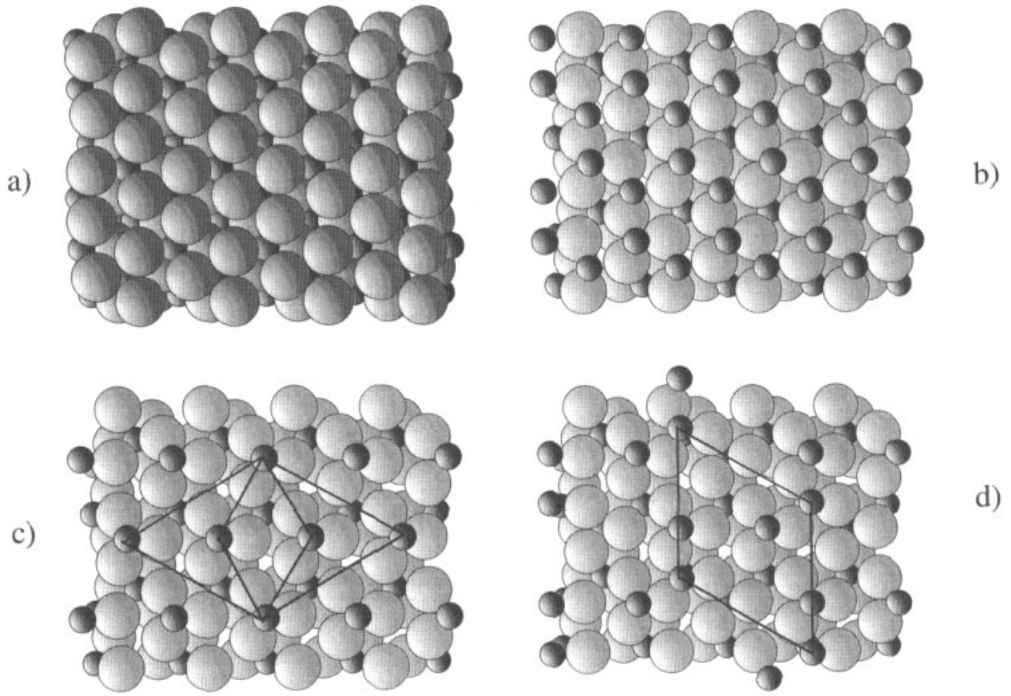

Figure 8. Three different terminations of the chromium oxide surface: (a) by a close oxygen atom layer; (b) by a full chromium ion layer; (c) by half a chromium ion layer, where unit meshes (1×1) and $(\sqrt{3} \times \sqrt{3})R30°$ are shown; (d) as (c), showing a third of the Cr^{3+} ions which have coherently hopped from site 1 to site 3, which gives rise to the indicated $(\sqrt{3} \times \sqrt{3})R30°$ unit mesh.

structure appears, indicating a larger unit cell. The low transition temperature of 150 K already provides evidence that the process is connected with a relatively low activation energy. As a rule of thumb, one would estimate activation energies in the range of 0.3 eV which would be consistent with surface diffusion processes. The kind of structure resulting from such diffusion processes is indicated in figure 8(d). There are several reasons why such a structural rearrangement may take place.

Starting with the situation at the lowest temperature we believe that the Cr^{3+} ions are all in equivalent sites. These sites could be those also occupied in the bulk (site 1, figure 1). There are two more threefold sites (sites 2 and 3, in figure 1) which are available for occupation. One, of course, is the other site occupied in the bulk (site 2). It is characteristic for this site that there is never a Cr^{3+} ion in the second layer below the top oxygen layer. The second alternative is the site characterized by an open oxygen triangle (site 3). There are Cr^{3+} ions in the second layer below this site. The question is: which is the most stable site populated at the lowest temperature? Our EELS data in comparison with the theoretical calculations indicate that the outer Cr^{3+} sites (site 1) are occupied at the lowest temperature. Each surface Cr^{3+} ion has a direct counterpart in the next layer down. If we assume a magnetic coupling in the first layers similar to the bulk situation, then there is antiferromagnetic coupling to the second Cr layer of the order of 12 meV [26], but within the topmost layer the Cr ions are ferromagnetically or very weakly antiferromagnetically coupled as indicated in the figure. The magnetic coupling that is important in this case

is between the topmost Cr^{3+} layer and the one below the quasi-hexagonally packed O^{2-} layer. Locally, this means that two Cr^{3+} ions are exchange coupled via three oxygen ions, forming a Cr^{3+}–O–Cr^{3+} angle of approximately 85°. This situation is similar to a dinuclear Cr^{3+} complex where the transition-metal ions are bridged by three hydroxyl groups. In this latter case the exchange splitting has been measured to be 8 meV [27]. This energy has to be surmounted to decouple the ions magnetically. If the temperature is raised, half or less of the Cr^{3+} ions at the surface may be decoupled from the second layer and may change site. Consequently, a larger unit cell with a $(\sqrt{3} \times \sqrt{3})R30°$ unit mesh is observed. A schematic representation is shown in figure 8(d). As is revealed by the schematic drawing, the Cr^{3+} ions reside only in sites that have a second Cr^{3+} ion underneath in the second layer. There are basically two reasons for this. Primarily, the thermal dependence of the EEL spectra is consistent with this occupation. The intensities of the surface peaks A and B decrease, indicating that the occupation of site 1 is reduced. Since site 2 is not stable with respect to the motion of the Cr^{3+} through the oxygen plane into the second layer, the Cr^{3+} ions can only move to the stable site 3. Secondly, there is an antiferromagnetic coupling among the Cr^{3+} ions in each Cr layer, which is about half that through the Cr–O_3–Cr bridge [27]. Therefore, each ion is antiferromagnetically coupled within the top layer and also with respect to the second Cr^{3+} ion layer. Such effects may represent the driving force for the process to occur. The energy differences between differently magnetically coupled states are of the order of 6 meV [27], compatible with our temperature dependent EEL spectra.

At higher temperatures the two different Cr^{3+} sites at the surface are statistically occupied, giving rise to a unit mesh typical of a lattice gas. This again leads to a $p(1 \times 1)$ structure with very diffuse intensity in the range of the $(\sqrt{3} \times \sqrt{3})R30°$ positions. This sequence of events would explain the observed changes in the diffraction patterns as well as the changes in the EEL spectra. The latter will be considered in more detail in the following. The key aspect is the exchange between the two inequivalent Cr^{3+} sites on the $Cr_2O_3(111)$ surface. We have shown that the inequivalent ligand fields for the two sites lead to different d–d excitation energies. Therefore the d–d transitions in the EEL spectra may be used to follow the site exchange process. Figure 7 shows at the lowest temperature a d–d spectrum which is compatible with the spectrum calculated for the Cr^{3+} ion site 1. We assume that the magnetic exchange with the second layer favours this geometry. Upon heating the surface we propose that site 3 becomes populated. This is documented by a redistribution of intensity in the sense that the peak at 1.4 eV is washed out at the expense of the feature at 1.75 eV which appears to become broader. In comparison with the calculated energies we see that the ^4E and $^4A_1$ states at the lowest excitation energies are close in energy and contribute to the leading peak but reduce the intensity of the second peak. The two $^4A_2$ and ^4E states at higher energies are, however, lower than the corresponding excitations for the Cr^{3+} ions in site 1, thus leading to an increase in the width of feature C. It is thus clear that the changes observed in the EEL spectra are fully compatible with the proposed changes in the LEED patterns. Also, the observed order-to-order transition behaviour towards low temperatures and the order-to-disorder transition behaviour towards high temperatures is fully in line with the observation.

7. Conclusion

We report the surface structure rearrangements in the system $Cr_2O_3(111)/Cr(110)$ upon temperature variation between 90 and 300 K. The rearrangement was immediately quenched

by the adsorption of carbon dioxide and oxygen, respectively. Thus the processes involved very probably take place in the very first layer of the oxide surface rather than throughout the whole oxide lattice.

EEL spectra also showed considerable changes in two signals over the above-mentioned temperature interval. These signals are assigned to d–d transitions on surface chromium species by their sensitivity to adsorbates. The observed intensity changes in the temperature interval between 90 and 440 K suggest the surface chromium ions to be directly involved in the surface rearrangement processes.

We propose a two-step model of an order-to-order transition below 150 K, followed by an order-to-disorder transition of the surface chromium ion spins above 150 K. The latter may be driven by antiferromagnetic coupling of the spins to those of the chromium ions in the second layer. The antiferromagnetic coupling is suggested to lead to a lattice distortion which then becomes observable in LEED. An estimation of the energy difference for the phase transition yields a value of about 10 meV which is of the order of magnitude for weak antiferromagnetic coupling.

Acknowledgments

We gratefully acknowledge the discussion contributions of K Heinz, Erlangen, and P Chaudhuri, Bochum. For the drawings we thank Heiko Schlienz and Thomas Risse. Our research has been supported by several agencies: Deutsche Forschungsgemeinschaft, Bundesministerium für Bildung, Wissenschaft, Forschung und Technologie (BMBF), Ministerium für Wissenschaft und Forschung des Landes Nordrhein–Westfalen, European Communities (Brite–Euram) and Fond der chemischen Industrie. We are grateful for their support.

References

[1] Henrich V E and Cox P A 1994 *The Surface Science of Metal Oxides* (Cambridge: Cambridge University Press)
[2] Freund H-J and Umbach E 1993 *Adsorption on Ordered Surfaces of Ionic Solids and Thin Films (Springer Series in Surface Science 33)* (Berlin: Springer)
[3] Scarano D, Spoto G, Bordiga S, Carnelli L, Ricchardi G and Zecchina A 1994 *Langmuir* **10** 3094
[4] Kuhlenbeck H and Freund H-J 1993 *Springer Proceedings in Physics* vol 73, ed R F Howe, R N Lamb and K Wandelt (Berlin: Springer)
[5] Rohr F, Wirth K, Libuda J, Bäumer M and Freund H-J 1994 *Surf. Sci.* **315** L2977, and references therein
[6] Xu C, Haßel M, Kuhlenbeck H and Freund H-J 1991 *Surf. Sci.* **258** 23
[7] Kuhlenbeck H *et al* 1992 *Ber. Bunsenges. Phys. Chem.* **96** 15
[8] Haßel M 1991 *Diploma Thesis* Ruhr-Universität Bochum
[9] Al-Shamery K, Beauport I, Freund H-J and Zacharias H 1994 *Chem. Phys. Lett.* **222** 107
Wilde M 1994 *Diploma Thesis* Ruhr-Universität Bochum
[10] Roth W L 1960 *J. Appl. Phys.* **31** 2000
[11] Rooksby H P 1948 *Acta Crystallogr.* **1** 226
Greenwald S and Smart J S 1950 *Nature* **166** 523
Kanamori J 1957 *Prog. Theor. Phys.* **17** 197
[12] Menges M 1993 *Thesis* Ruhr-University Bochum
[13] Jaeger R M, Kuhlenbeck H and Freund H-J 1993 *Chem. Phys. Lett.* **203** 41
[14] Kennett H M and Lee A E 1972 *Surf. Sci.* **33** 377
Michel P and Jardin C 1973 *Surf. Sci.* **36** 478
[15] Ekelund S and Leygraf C 1973 *Surf. Sci.* **40** 179
[16] Forster L S 1990 *Chem. Rev.* **90** 331

[17] Allos T I Y, Birss R R, Parker M R, Ellis E and Johnson D W 1977 *Solid State Commun.* **24** 129
[18] Schawlow A L, Wood D L and Clogston A M 1959 *Phys. Rev. Lett.* **3** 271
[19] Kuhlenbeck H 1994 *Appl.Phys.* A **59** 469
[20] Wyckoff R W G 1963 *Crystal Structures* vol I, 2nd edn (New York: Wiley–Interscience)
[21] Freitag A, Staemmler V, Cappus D, Ventrice C A Jr, Al-Shamery K, Kuhlenbeck H and Freund H-J 1993 *Chem. Phys. Lett.* **210** 10
[22] Haßel M, Kuhlenbeck H, Freund H-J, Shi S, Freitag A, Staemmler V, Lütkehoff S and Neumann M 1995 *Chem. Phys. Lett.* submitted
[23] Shi S and Staemmler V 1995 submitted
[24] Ehrlich D, Staemmler V and Freund H-J 1995 to be published
[25] Tasker P W 1984 *Advances in Ceramics* vol 10, ed W D Kingery (Columbus, OH: American Ceramic Society)
[26] Samuelsen E J, Hutchings M T and Shirane G 1970 *Physica* **48** 13
[27] Riesen H and Güdel H U 1987 *Mol. Phys.* **60** 1221